

---

# Accelerating Universe: Observational Status and Theoretical Implications

L. Perivolaropoulos

Department of Physics, University of Ioannina, Greece  
e-mail: leandros@cc.uoi.gr

This is a pedagogical review of the recent observational data obtained from type Ia supernova surveys that support the accelerating expansion of the universe. The methods for the analysis of the data are reviewed and the theoretical implications obtained from their analysis are discussed.

## 1 Introduction

Recent distance-redshift surveys [1, 2, 3, 4, 5, 6] of cosmologically distant Type Ia supernovae (SnIa) have indicated that the universe has recently (at redshift  $z \approx 0.5$ ) entered a phase of accelerating expansion. This expansion has been attributed to a dark energy [7] component with negative pressure which can induce repulsive gravity and thus cause accelerated expansion. The evidence for dark energy has been indirectly verified by Cosmic Microwave Background (CMB) [8] and large scale structure [9] observations.

The simplest and most obvious candidate for this dark energy is the cosmological constant [10] with equation of state  $w = p = -1$ . The extremely fine tuned value of the cosmological constant required to induce the observed accelerated expansion has led to a variety of alternative models where the dark energy component varies with time. Many of these models make use of a homogeneous, time dependent minimally coupled scalar field (quintessence [11, 12]) whose dynamics is determined by a specially designed potential  $V(\phi)$  inducing the appropriate time dependence of the field equation of state  $w(z) = \frac{p(\phi)}{\rho(\phi)}$ . Given the observed  $w(z)$ , the quintessence potential can in principle be determined. Other physically motivated models predicting late accelerated expansion include modified gravity [13, 14, 15], Chaplygin gas [16], Cardassian cosmology [17], theories with compactified extra dimensions [18, 19], braneworld models [20] etc. Such cosmological models predict specific forms of the Hubble parameter  $H(z)$  as a function of redshift  $z$ . The observational determination of the recent expansion history  $H(z)$  is therefore important for the identification of the viable cosmological models.

The most direct and reliable method to observationally determine the recent expansion history of the universe  $H(z)$  is to measure the redshift  $z$  and the apparent luminosity of cosmological distant indicators (standard candles) whose absolute luminosity is known. The luminosity distance vs. redshift is thus obtained which in turn leads to the Hubble expansion history  $H(z)$ .

The goal of this review is to present the methods used to construct the recent expansion history  $H(z)$  from SNIa data and discuss the most recent observational results and their theoretical implications. In the next section I review the method used to determine  $H(z)$  from cosmological distance indicators and discuss SNIa as the most suitable cosmological standard candles. In section 3 I show the most recent observational results for  $H(z)$  and discuss their possible interpretations other than accelerating expansion. In section 4 I discuss some of the main theoretical implications of the observed  $H(z)$  with emphasis on the various parametrizations of dark energy (the simplest being the cosmological constant). The best fit parametrizations are shown and their common features are pointed out. The physical origin of models predicting the best fit form of  $H(z)$  is discussed in section 5 where I distinguish between minimally coupled scalar fields (quintessence) and modified gravity theories. An equation of state of dark energy with  $w < -1$  is obtained by a specific type of dark energy called phantom energy [21]. This type of dark energy is faced with theoretical challenges related to the stability of the theories that predict it. Since however the SNIa data are consistent with phantom energy it is interesting to investigate the implications of such an energy. These implications are reviewed in section 6 with emphasis to the Big Rip future singularity implied by such models as the potential death of the universe. Finally, in section 7 I review the future observational and theoretical prospects related to the investigation of the physical origin of dark energy and summarize the main conclusions of this review.

## 2 Expansion History from the Luminosity Distances of SNIa

Consider a luminous cosmological object emitting at total power  $L$  (absolute luminosity) in radiation within a particular wavelength band. Consider also an observer (see Fig. 1) at a distance  $d_L$  from the luminous object. In a static cosmological setup, the power radiated by the luminous object is distributed in the spherical surface with radius  $d_L$  and therefore the intensity  $l$  (apparent luminosity) detected by the observer is

$$l = \frac{L}{4 d_L^2} \quad (1)$$

The quantity

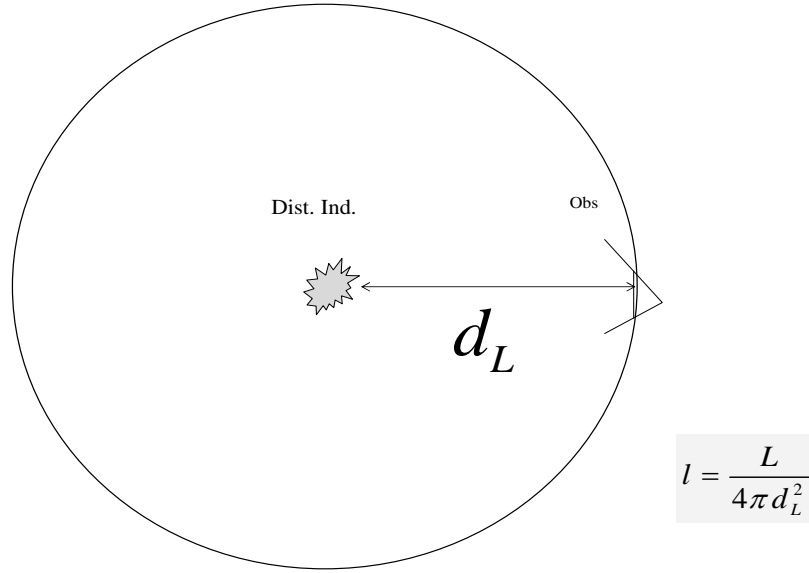


Fig. 1. The luminosity distance obtained from the apparent and absolute luminosities

$$d_L = \frac{r}{\frac{L}{4\pi l}} \tag{2}$$

is known as the luminosity distance to the luminous object and in a static universe it coincides with the actual distance. In an expanding universe however, the energy of the radiation detected by the observer has been reduced not only because of the distribution of photons on the spherical surface but also because the energy of the photons has been redshifted while their detection rate is reduced compared to their emission rate due to the cosmological expansion [22]. Both of these expansion effects give a reduction of the detected energy by a factor  $\frac{a(t_0)}{a(t)} = (1+z)$  where  $a(t)$  is the scale factor of the universe at cosmic time  $t$  and  $t_0$  is the present time. Usually  $a$  is normalized so that  $a(t_0) = 1$ . Thus the detected apparent luminosity in an expanding background may be written as

$$l = \frac{L}{4 a(t_0)^2 x(z)^2 (1+z)^2} \tag{3}$$

where  $x(z)$  is the comoving distance to the luminous object emitting with redshift  $z$ . This implies that in an expanding universe the luminosity distance  $d_L(z)$  is related to the comoving distance  $x(z)$  by the relation

$$d_L(z) = x(z) (1+z) \tag{4}$$

Using eq. (4) and the fact that light geodesics in a flat expanding background obey

$$c dt = a(z) dx(z) \quad (5)$$

it is straightforward to eliminate  $x(z)$  and express the expansion rate of the universe  $H(z) = \frac{\dot{a}}{a}(z)$  at a redshift  $z$  (scale factor  $a = \frac{1}{1+z}$ ) in terms of the observable luminosity distance as

$$H(z) = c \left[ \frac{d}{dz} \left( \frac{d_L(z)}{1+z} \right) \right]^{-1} \quad (6)$$

This is an important relation that connects the theoretically predictable Hubble expansion history  $H(z)$  with the observable luminosity distance  $d_L(z)$  in the context of a spatially flat universe. Therefore, if the absolute luminosity of cosmologically distant objects is known and their apparent luminosity is measured as a function of redshift, eq. (2) can be used to calculate their luminosity distance  $d_L(z)$  as a function of redshift. The expansion history  $H(z)$  can then be deduced by differentiation with respect to the redshift using eq. (6). Conversely, if a theoretically predicted  $H(z)$  is given, the corresponding predicted  $d_L(z)$  is obtained from (6) by integrating  $H(z)$  as

$$d_L(z) = c (1+z) \int_0^z \frac{dz'}{H(z')} \quad (7)$$

This predicted  $d_L(z)$  can be compared with the observed  $d_L(z)$  to test the consistency of the theoretical model with observations. In practice astronomers do not refer to the ratio of absolute over apparent luminosity. Instead they use the difference between apparent magnitude  $m$  and absolute magnitude  $M$  which is connected to the above ratio by the relation

$$m - M = 2.5 \log_{10} \left( \frac{L}{L_\odot} \right) \quad (8)$$

A particularly useful diagram which illustrates the expansion history of the Universe is the Hubble diagram. The x-axis of a Hubble diagram (see Fig. 2) shows the redshift  $z$  of cosmological luminous objects while the y-axis shows the physical distance  $r$  to these objects. In the context of a cosmological setup the redshift  $z$  is connected to the scale factor  $a(t)$  at the time of emission of radiation by  $1+z = \frac{a(t_0)}{a(t)}$  where  $t_0$  is the present time. On the other hand, the distance to the luminous object is related to the time in the past  $t_{\text{past}}$  when the radiation emission was made. Therefore, the Hubble diagram contains information about the time dependence of the scale factor  $a(t)$ . The slope of this diagram at a given redshift denotes the inverse of the expansion rate  $\frac{\dot{a}}{a}(z) = H(z)$  i.e.

$$r = \frac{1}{H(z)} c z \quad (9)$$

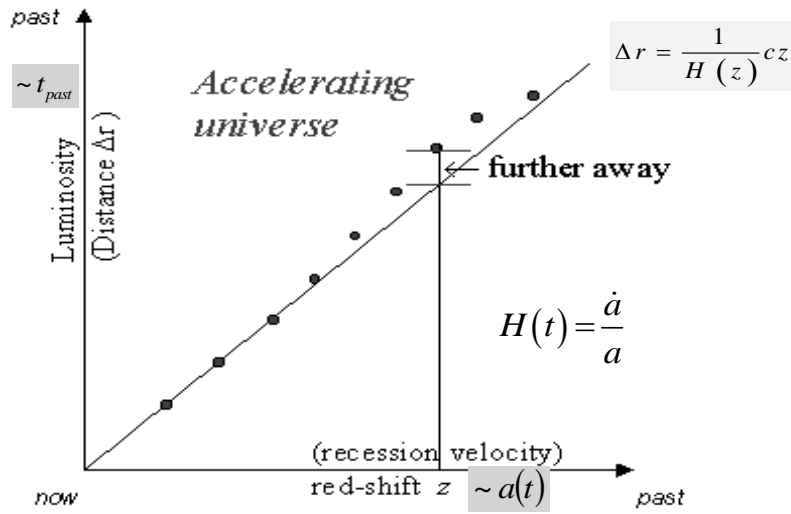


Fig. 2. The Hubble diagram. In an accelerating universe luminous objects at a given redshift appear to be dimmer.

In an accelerating universe the expansion rate  $H(z)$  was smaller in the past (high redshift) and therefore the slope  $H^{-1}$  of the Hubble diagram is larger at high redshift. Thus, at given redshift, luminous objects appear to be further away (dimmer) compared to an empty universe expanding with a constant rate (see Fig. 2).

The luminous objects used in the construction of the Hubble diagram are objects whose absolute luminosity is known and therefore their distance can be evaluated from their apparent luminosity along the lines discussed above. Such objects are known as distance indicators or standard candles. A list of common distance indicators used in astrophysics and cosmology is shown in Table 1 along with the range of distances where these objects are visible and the corresponding accuracy in the determination of their absolute magnitude. As shown in Table 1 the best choice distance indicators for cosmology are  $S_nIa$  not only because they are extremely luminous (at their peak they are as luminous as a bright galaxy) but also because their absolute magnitude can be determined at a high accuracy.

Type Ia supernovae emerge in binary star systems where one of the companion stars has a mass below the Chandrasekhar limit  $1.4M_{\odot}$  and therefore ends up (after hydrogen and helium burning) as white dwarf supported by degeneracy pressure. Once the other companion reaches its red giant phase the white dwarf begins gravitational stripping of the outer envelope of the red giant thus accreting matter from the companion star. Once the white dwarf

Table 1. Extragalactic distance indicators (from Ref. [23])

Technique	Range of distance	Accuracy (1 $\sigma$ )
Cepheids	< LM C to 25 M pc	0.15 mag
SN Ia	4 M pc to > 2 G pc	0.2 mag
Expand. Phot. Meth./SnII LM C	to 200 M pc	0.4 mag
Planetary Nebulae	LM C to 20 M pc	0.1 mag
Surf. Brightness Fluct	1 M pc to 100 M pc	0.1 mag
Tully Fisher	1 M pc to 100 M pc	0.3 mag
Brightest Cluster Gal.	50 M pc to 1 G pc	0.3 mag
Glob. Cluster Lum. Fun.	1 M pc to 100 M pc	0.4 mag
Sunyaev-Zeldovich	100 M pc to > 1 G pc	0.4 mag
Gravitational Lensing	5 G pc	0.4 mag

reaches a mass equal to the Chandrasekhar limit, the degeneracy pressure is unable to support the gravitational pressure, the white dwarf shrinks and increases its temperature igniting carbon fusion. This leads to violent explosion which is detected by a light curve which rapidly increases luminosity in a time scale of less than a month, reaches a maximum and disappears in a timescale of 1-2 months (see Fig. 3). Type Ia are the preferred distance indicators for

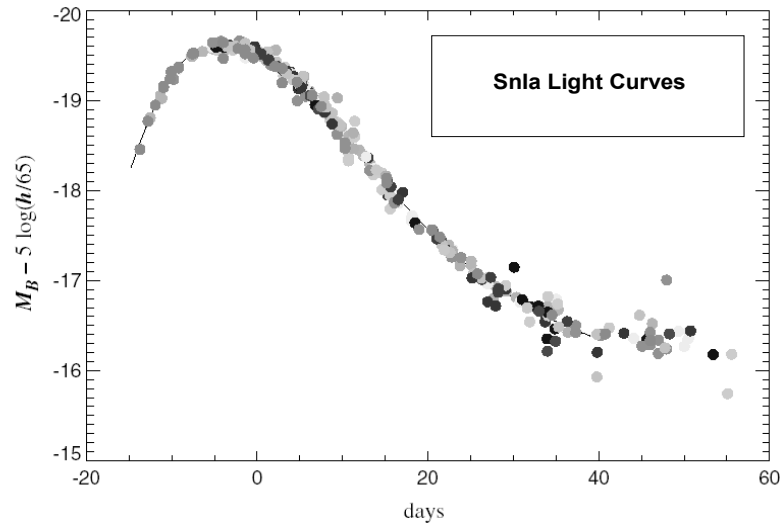


Fig. 3. Typical SnIa light-curve.

cosmology for several reasons:

1. They are exceedingly luminous. At their peak luminosity they reach an absolute magnitude of  $M \approx -19$  which corresponds to about  $10^{10} M_{\odot}$ .
2. They have a relatively small dispersion of peak absolute magnitude.
3. Their explosion mechanism is fairly uniform and well understood.
4. There is no cosmic evolution of their explosion mechanism according to known physics.
5. There are several local SNIa to be used for testing SNIa physics and for calibrating the absolute magnitude of distant SNIa.

On the other hand, the main problem for using SNIa as standard candles is that they are not easy to detect and it is impossible to predict a SNIa explosion. In fact the expected number of SNIa exploding per galaxy is 1-2 per millennium. It is therefore important to develop a search strategy in order to efficiently search for SNIa at an early stage of their light curve. The method used (with minor variations) to discover and follow up photometrically and spectroscopically SNIa consists of the following steps [1, 2, 3, 4]:

1. Observe a number of wide fields of apparently empty sky out of the plane of our Galaxy. Tens of thousands of galaxies are observed in a few patches of sky.
2. Come back three weeks later (next new moon) to observe the same galaxies over again.
3. Subtract images to identify on average 12-14 SNIa.
4. Schedule in advance follow up photometry and spectroscopy on these SNIa as they brighten to peak and fade away.

Given the relatively short time difference (three weeks) between first and second observation, most SNIa do not have time to reach peak brightness so almost all the discoveries are pre-maximum. This strategy turns a rare, random event into something that can be studied in a systematic way. This strategy is illustrated in Figs 4 and 5 (from Ref. [24]). The outcome of this observation strategy is a set of SNIa light curves in various bands of the spectrum (see Fig. 6). These light curves are very similar to each other and their peak apparent luminosity could be used to construct the Hubble diagram assuming a common absolute luminosity.

Before this is done however a few corrections must be made to take into account the minor intrinsic absolute luminosity differences (due to composition differences) among SNIa as well as the radiation extinction due to the intergalactic medium. Using samples of closeby SNIa it has been empirically observed that the minor differences of SNIa absolute luminosity are connected with differences in the shape of their light curves. Broad slowly declining light curves (stretch factor  $s > 1$ ) correspond to brighter SNIa while narrower rapidly declining light curves (stretch factor  $s < 1$ ) correspond to intrinsically fainter SNIa. This stretch factor dependence of the SNIa absolute luminosity has been verified using closeby SNIa [26] It was shown that contraction of broad light curves while reducing peak luminosity and stretching narrow light

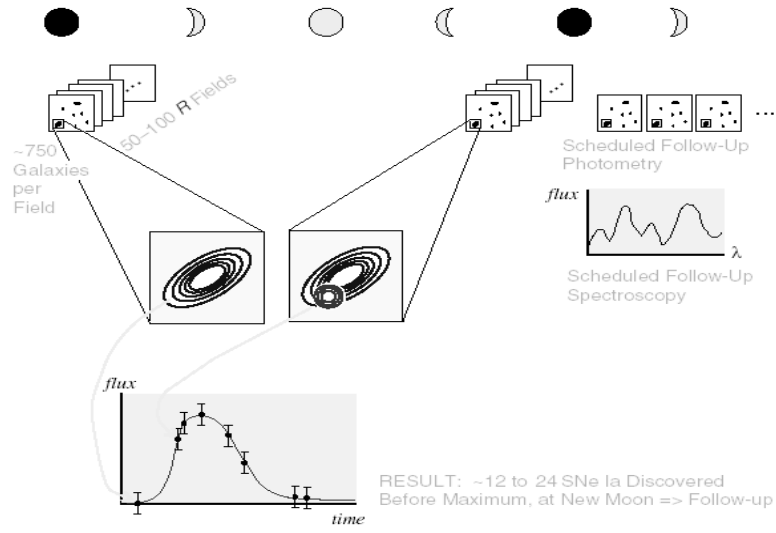


Fig. 4. Search strategy to discover of supernovae in a scheduled, systematic procedure [24]

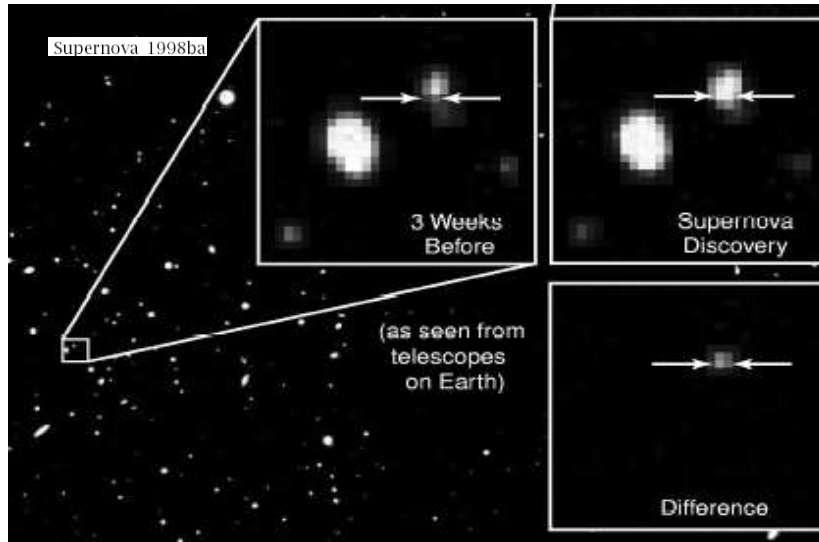


Fig. 5. Supernova 1998ba, an example of a supernova discovery using the search strategy described in the text involving subtraction of images.



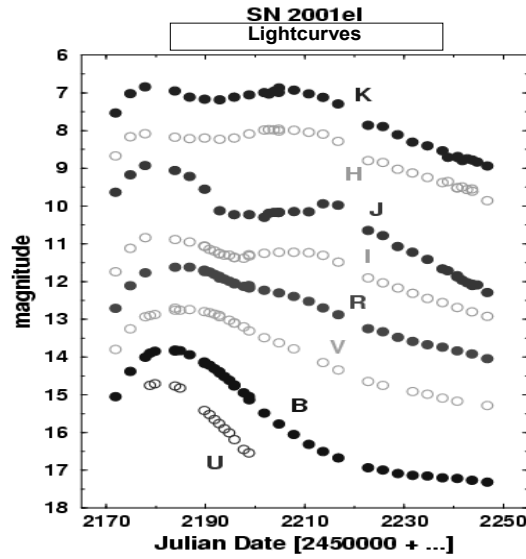


Fig. 6. A set of light curves from SN 2001el in various bands of the spectrum .

curves while increasing peak luminosity makes these light curves coincide (see Fig. 7). In addition to the stretch factor correction an additional correction must be made in order to compare the light curves of high redshift SNIa with those of lower redshift. In particular all light curves must be transformed to the same reference frame and in particular the rest frame of the SNIa. For example a low redshift light curve of the blue B band of the spectrum should be compared with the appropriate red R band light curve of a high redshift SNIa. The transformation also includes correction for the cosmic time dilation (events at redshift  $z$  last  $1+z$  times longer than events at  $z=0$ ). These corrections consist the K-correction and is used in addition to the stretch factor correction discussed above. The K-correction transformation is illustrated in Fig. 8.

### 3 Observational Results

The first project in which SNIa were used to determine the cosmological constant energy was the research from Perlmutter et al. in 1997 [26]. The project was known as the Supernova Cosmology Project (SCP). Applying the above described methods they discovered seven distant SNIa at redshift  $0.35 < z < 0.65$ . When discovered, the supernovae were followed for a year by different telescopes on earth to obtain good photometry data in different bands, in order to measure good magnitudes. The Hubble diagram they

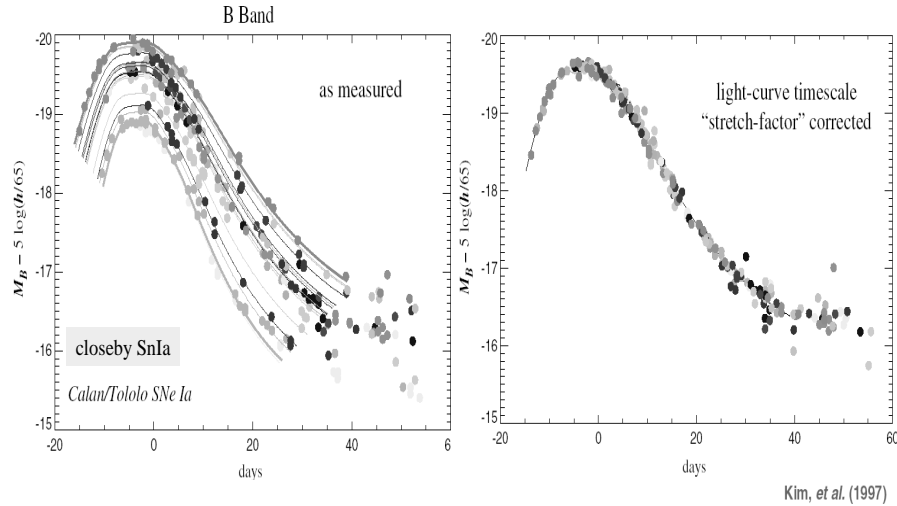


Fig. 7. Left: The range of lightcurve for low-redshift supernovae discovered by the Calan/Tololo Supernova Survey. At these redshifts, the relative distances can be determined (from redshift), so their relative brightnesses are known. Right: The same lightcurves after calibrating the supernova brightness using the stretch of the timescale of the lightcurve as an indicator of brightness (and the color at peak as an indicator of dust absorption)

constructed was consistent with standard Friedmann cosmology without dark energy or cosmological constant.

A year after their first publication, Perlmutter et al. published in Nature [1] an update on their initial results. They had included the measurements of a very high-redshifted  $z = 0.83$  Supernova Ia. This dramatically changed their conclusions. The standard decelerating Friedmann cosmology was ruled out at about 99% confidence level. The newly discovered Supernova indicated a universe with accelerating expansion dominated by dark energy. These results were confirmed independently by another pioneer group (High- $z$  Supernova Search Team (HST)) searching for SNIa and measuring the expansion history  $H(z)$  (Riess et al. in 1998 [2]). They had discovered 16 SNIa at  $0.16 < z < 0.62$  and their  $H(z)$  also indicated accelerating expansion ruling out for a flat universe. Their data also permitted them to definitely rule out decelerating Friedmann cosmology at about 99% confidence level.

In 2003 Tonry et al. [3] reported the results of their observations of eight newly discovered SNIa. These SNIa were found in the region  $0.3 < z < 1.2$ . Together with previously acquired SNIa data they had a data set of more than 100 SNIa. This dataset confirmed the previous findings of accelerated expansion.

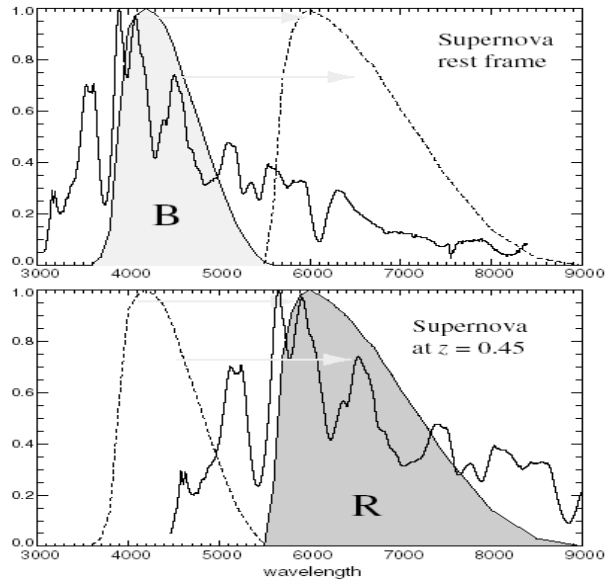


Fig. 8. Slightly different parts of the supernova spectrum are observed through the B filter transmission function at low redshift (upper panel) and through the R filter transmission function at high redshift (lower panel). This small difference is accounted for by the cross-filter K-correction [25].

sion and gave the first hints of decelerated expansion at redshifts  $z > 0.6$  when matter is expected to begin dominating over dark energy. This transition from decelerating to accelerating expansion was confirmed and pinpointed accurately by Riess et al. in 2004 [5] who included in the analysis 16 new high-redshift SNIa obtained with HST and reanalyzed all the available data in a uniform and robust manner constructing a robust and reliable dataset consisting of 157 points known as the Gold dataset. These SNIa included 6 of the 7 highest redshift SNIa known with  $z > 1.25$ . With these new observations, they could clearly identify the transition from a decelerating towards an accelerating universe to be at  $z = 0.46 \pm 0.13$ . It was also possible to rule out the effect of dust on the dimming of distant SNIa, since the accelerating/decelerating transition makes the effect of dimming inverse. The Hubble diagram obtained from the Gold dataset is shown in Fig. 9 where the corrected apparent magnitude  $m(z)$  of the 157 SNIa is plotted versus the redshift  $z$ . The apparent magnitude  $m(z)$  is related to the corresponding luminosity distance  $d_L$  of the SNIa by

$$m(z) = M + 5 \log_{10} \left[ \frac{d_L(z)}{M \text{ pc}} \right] + 25 \tag{10}$$

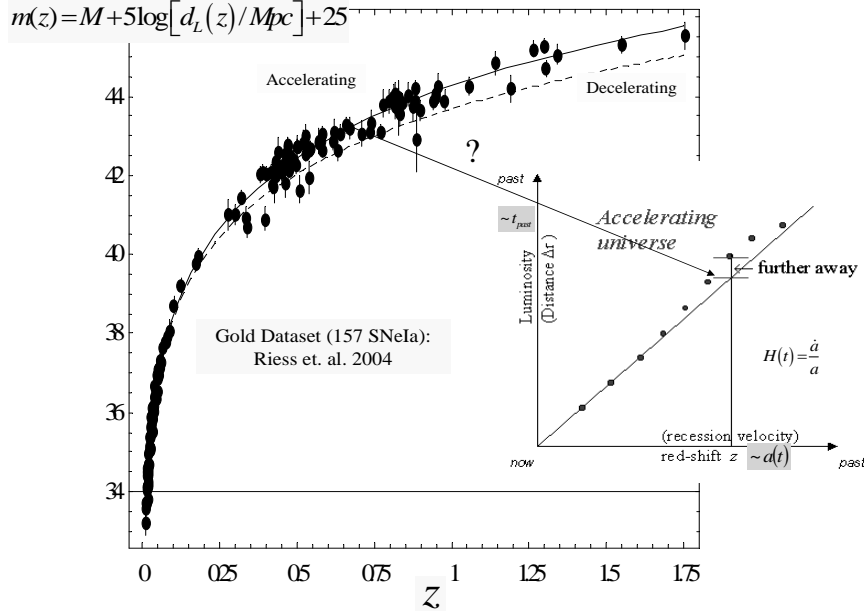


Fig. 9. The apparent magnitude  $m(z)$  vs redshift as obtained from the Gold dataset. It is not easy to distinguish between accelerating and decelerating expansion in such a diagram.

where  $M$  is the absolute magnitude which is assumed to be constant for standard candles like SNIa after the corrections discussed in section 2 are implemented.

A potential problem of plots like the one of Fig. 9 is that it is not easy to tell immediately if the data favor an accelerating or decelerating universe. This would be easy to tell in the Hubble diagram of Fig. 2 where the distance is plotted vs redshift and is superposed with the distance-redshift relation  $d_L^{\text{empty}}(z)$  of an empty universe with  $H(z)$  constant. An even more efficient plot for such a purpose would be the plot of the ratio  $\frac{d_L(z)}{d_L^{\text{empty}}(z)}$  (or its  $\log_{10}$ ) which can immediately distinguish accelerating from decelerating expansion by comparing with the  $\frac{d_L(z)}{d_L^{\text{empty}}(z)} = 1$  line. Such a plot is shown in Fig. 10 [5] using both the raw Gold sample data and the same data binned in redshift bins.

The lines of zero acceleration, constant acceleration and constant deceleration are also shown for comparison. Clearly the best fit is obtained by an expansion which is accelerating at recent times ( $z < 0.5$ ) and decelerating at earlier times ( $z > 0.5$ ) when matter is expected to dominate.

The interpretation of the data assuming that the observed dimming at high redshift is due to larger distance may not be the only possible interpretation. The most natural alternative interpretations however have been shown to lead

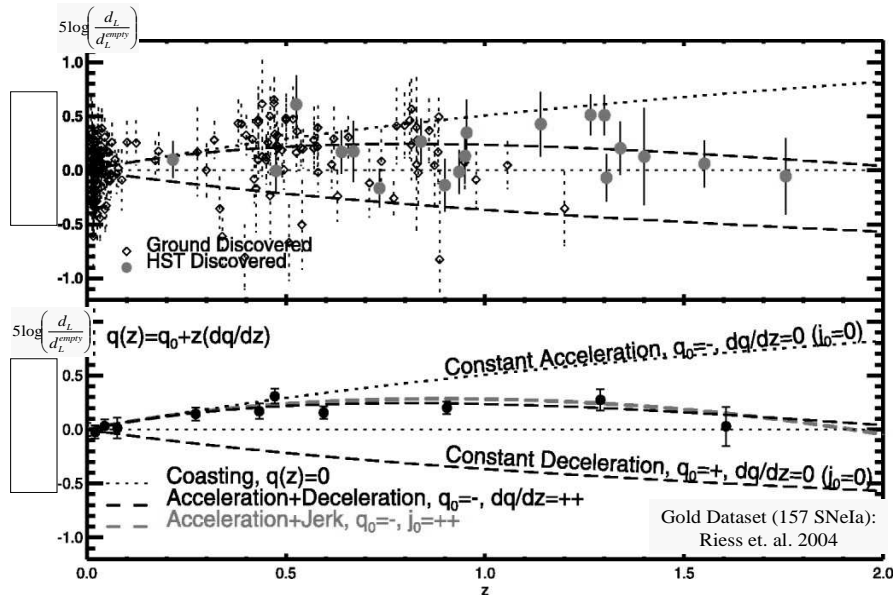


Fig. 10. The reduced Hubble diagram used to distinguish between accelerating and decelerating expansion [5].

to inconsistencies and none of them has been favored as a viable alternative at present. These alternative interpretations include the following:

**Intergalactic Dust:** Ordinary astrophysical dust does not obscure equally at all wavelengths, but scatters blue light preferentially, leading to the well-known phenomenon of "reddening". Spectral measurements [5] reveal a negligible amount of reddening, implying that any hypothetical dust must be a novel "grey" variety inducing no spectral distortions [27].

**Grey Dust:** Grey dust is highly constrained by observations: first, it predicts further increase of dimming at higher redshifts  $z > 0.5$  which is not observed; and second, intergalactic dust would absorb ultraviolet/optical radiation and re-emit it at far infrared wavelengths, leading to stringent constraints from observations of the cosmological far-infrared background. Thus, while the possibility of obscuration has not been entirely eliminated, it requires a novel kind of dust which is already highly constrained (and may be convincingly ruled out by further observations).

**Evolution of SNIa:** The supernova search teams have found consistency in the spectral and photometric properties of SNIa over a variety of redshifts and environments [5] (e.g., in elliptical vs. spiral galaxies). Thus despite the relevant tests there is currently no evidence that the observed dimming can be attributed to evolution of SNIa.

According to the best of our current understanding, the supernova results indicating an accelerating universe seem likely to be trustworthy. Needless to say, however, the possibility of a neglected systematic effect can not be definitively excluded. Future experiments, discussed in section 7 will both help us improve our understanding of the physics of supernovae and allow a determination of the distance/redshift relation to sufficient precision to distinguish between the effects of an accelerating universe and those of possible astrophysical phenomena.

#### 4 Dark Energy and Negative Pressure

Our current knowledge of the expansion history of the universe can be summarized as follows: The universe originated at an initial state that was very close to a density singularity known as the Big Bang. Soon after that it entered a phase of superluminal accelerating expansion known as inflation. During inflation causally connected regions of the universe exited out of the horizon, the universe approached spatial flatness and the primordial fluctuations that gave rise to structure were generated. At the end of inflation the universe was initially dominated by radiation and later by matter whose attractive gravitational properties induced a decelerating expansion.

The SNIa data discussed in section 3 (along with other less direct cosmological observations [8, 9]) strongly suggest that the universe has recently entered a phase of accelerating expansion at a redshift  $z \approx 0.5$ . This accelerating expansion can not be supported by the attractive gravitational properties of regular matter. The obvious question to address is therefore ‘What are the properties of the additional component required to support this acceleration?’. To address this question we must consider the dynamical equation that determines the evolution of the scale factor  $a(t)$ . This equation is the Friedmann equation which is obtained by combining General Relativity with the cosmological principle of homogeneity and isotropy of the universe. It may be written as

$$\frac{\ddot{a}}{a} = -\frac{4\pi G}{3} \sum_i (\rho_i + 3p_i) = -\frac{4\pi G}{3} [\rho_m + (\rho_x + 3p_x)] \quad (11)$$

where  $\rho_i$  and  $p_i$  are the densities and pressures of the contents of the universe assumed to behave as ideal fluids. The only directly detected fluids in the universe are matter ( $\rho_m; p_m = 0$ ) and the subdominant radiation ( $\rho_r; p_r = -\rho_r/3$ ). Both of these fluids are unable to cancel the minus sign on the rhs of the Friedmann equation and can therefore only lead to decelerating expansion. An accelerating expansion in the context of general relativity can only be obtained by assuming the existence of an additional component ( $\rho_x; p_x = w_x \rho_x$ ) termed ‘dark energy’ which could potentially change the minus sign of eq. (11) and thus lead to accelerating expansion. Assuming a positive energy density for

dark energy (required to achieve atness) it becomes clear that negative pressure is required for accelerating expansion. In fact, writing the Friedm an eq. (11) in terms of the dark energy equation of state parameter  $w$  as

$$\frac{\ddot{a}}{a} = \frac{4}{3} \frac{G}{a^3} [\rho_m + \rho_x (1 + 3w)] \tag{12}$$

it becomes clear that a  $w < -\frac{1}{3}$  is required for accelerating expansion implying repulsive gravitational properties for dark energy.

The redshift dependence of the dark energy can be easily connected to the equation of state parameter  $w$  by combining the energy conservation  $d(\rho_x a^3) = -p_x d(a^3)$  with the equation of state  $p_x = w \rho_x$  as

$$\rho_x a^{3(1+w)} = (1+z)^{3(1+w)} \tag{13}$$

This redshift dependence is related to the observable expansion history  $H(z)$  through the Friedm an equation

$$H(z)^2 = \frac{\ddot{a}^2}{a^2} = \frac{8}{3} \frac{G}{a^3} [\rho_{0m} (\frac{a_0}{a})^3 + \rho_x(a)] = H_0^2 [\Omega_{0m} (1+z)^3 + \Omega_x(z)] \tag{14}$$

where the density parameter  $\Omega_{0crit}$  for matter is constrained by large scale structure observations to a value (prior)  $\Omega_{0m} \approx 0.3$ . Using this prior, the dark energy density parameter  $\Omega_x(z) = \frac{\rho_x(z)}{\rho_{0crit}}$  and the corresponding equation of state parameter  $w$  may be constrained from the observed  $H(z)$ .

In addition to  $\Omega_x(z)$ , the luminosity distance-redshift relation  $d_L(z)$  obtained from SNIa observations can constrain other cosmological parameters. The only parameter however obtained directly from  $d_L(z)$  (using eq. (6)) is the Hubble parameter  $H(z)$ . Other cosmological parameters can be obtained from  $H(z)$  as follows:

The age of the universe  $t_0$  is obtained as:

$$t_0 = \int_0^Z \frac{dz}{(1+z)H(z)} \tag{15}$$

The present Hubble parameter  $H_0 = H(z=0)$ .

The deceleration parameter  $q(z) = \frac{\ddot{a}a}{\dot{a}^2}$

$$q(z) = (1+z) \frac{d \ln H}{dz} - 1 \tag{16}$$

and its present value  $q_0 = q(z=0)$ .

The density parameters for matter and dark energy are related to  $H(z)$  through the Friedm an equation (14).

The equation of state parameter  $w(z)$  obtained as [28, 29]

$$w(z) = \frac{p_x(z)}{\rho_x(z)} = \frac{\frac{2}{3}(1+z) \frac{d \ln H}{dz} - 1}{1 - (\frac{H_0}{H})^2 \Omega_{0m} (1+z)^3} \tag{17}$$

obtained using the Friedm an equations (12) and (14).

The most interesting parameter from the theoretical point of view (apart from  $H(z)$  itself) is the dark energy equation of state parameter  $w(z)$ . This parameter probes directly the gravitational properties of dark energy which are predicted by theoretical models. The downside of it is that it requires two differentiations of the observable  $d_L(z)$  to be obtained and is therefore very sensitive to observational errors.

The simplest form of dark energy corresponds to a time independent energy density obtained when  $w = -1$  (see eq. (13)). This is the well known cosmological constant which was first introduced by Einstein in 1917 two years after the publication of the General Relativity (GR) equation

$$G = T \quad (18)$$

where  $\Lambda = 8\pi G/c^2$ . At the time the 'standard' cosmological model was a static universe because the observed stars of the Milky Way were found to have negligible velocities. The goal of Einstein was to apply GR in cosmology and obtain a static universe using matter only. It became clear that the attractive gravitational properties of matter made it impossible to obtain a static cosmology from (18). A repulsive component was required and at the time of major revolutions in the forms of physical laws it seemed more natural to obtain it by modifying the gravitational law than by adding new forms of energy density. The simplest generalization of eq. (18) involves the introduction of a term proportional to the metric  $g_{\mu\nu}$ . The GR equation becomes

$$G - \Lambda g_{\mu\nu} = T \quad (19)$$

where  $\Lambda$  is the cosmological constant. The repulsive nature of the cosmological constant becomes clear by the metric of a point mass (Schwarzschild-de Sitter metric) which, in the Newtonian limit leads to a gravitational potential

$$V(r) = -\frac{GM}{r} - \frac{\Lambda r^2}{6} \quad (20)$$

which in addition to the usual attractive gravitational term has a repulsive term proportional to the cosmological constant  $\Lambda$ . This repulsive gravitational force can lead to a static (but unstable) universe in a cosmological setup and in the presence of a matter fluid. A few years after the introduction of the cosmological constant by Einstein came Hubble's discovery that the universe is expanding and it became clear that the cosmological constant was an unnecessary complication of GR. It was then that Einstein (according to Gamow's autobiography) called the introduction of the cosmological constant 'the biggest blunder of my life'. In a letter to Lemaitre in 1947 Einstein wrote: 'Since I introduced this term I had always had a bad conscience. I am unable to believe that such an ugly thing is actually realized in nature'. As discussed below, there is better reason than ever before to believe that the cosmological constant may be non-zero, and Einstein may not have blundered after all.



If the cosmological constant is moved to the right hand side of eq. (19) it may be incorporated in the energy momentum tensor as an ideal fluid with  $\rho = \frac{\Lambda}{8\pi G}$  and  $w = -1$ . In the context of field theory such an energy momentum tensor is obtained by a scalar field with potential  $V(\phi)$  at its vacuum state  $\phi_0$  i.e.  $\dot{\phi} = 0$  and  $T_{\mu\nu} = -V(\phi_0)g_{\mu\nu}$ . Even though the cosmological constant may be physically motivated in the context of field theory and consistent with cosmological observation there are two important problems associated with it:

Why is it so incredibly small? Observationally, the cosmological constant density is 120 orders of magnitude smaller than the energy density associated with the Planck scale – the obvious cut-off. Furthermore, the standard model of cosmology posits that very early on the universe experienced a period of inflation: A brief period of very rapid acceleration, during which the Hubble constant was about 52 orders of magnitude larger than the value observed today. How could the cosmological constant have been so large then, and so small now? This is sometimes called the cosmological constant problem.

The 'coincidence problem': Why is the energy density of matter nearly equal to the dark energy density today?

Despite the above problems and given that the cosmological constant is the simplest dark energy model, it is important to investigate the degree to which it is consistent with the SNIa data. I will now describe the main steps involved in this analysis. According to the Friedmann equation the predicted Hubble expansion in a flat universe and in the presence of matter and a cosmological constant is

$$H(z)^2 = \frac{\dot{a}^2}{a^2} = \frac{8\pi G}{3} \rho_m \left(\frac{a_0}{a}\right)^3 + \frac{\Lambda}{3} = H_0^2 \left[ \Omega_m (1+z)^3 + \Omega_\Lambda \right] \quad (21)$$

where  $\Omega_m = \frac{\rho_m}{\rho_{crit}}$  and

$$\Omega_m + \Omega_\Lambda = 1 \quad (22)$$

This is the  $\Lambda$ CDM ( $\Lambda$  + Cold Dark Matter) which is currently the minimal standard model of cosmology. The predicted  $H(z)$  has a single free parameter which we wish to constrain by fitting to the SNIa luminosity distance-redshift data.

Observations measure the apparent luminosity vs redshift  $l(z)$  or equivalently the apparent magnitude vs redshift  $m(z)$  which are related to the luminosity distance by

$$2.5 \log_{10} \left( \frac{L}{l(z)} \right) = m(z) - M \quad 25 = 5 \log_{10} \left( \frac{d_L(z)_{obs}}{1 \text{ Mpc}} \right) \quad (23)$$

From the theory point of view the predicted observable is the Hubble parameter (21) which is related to the theoretically predicted luminosity distance

$d_L(z)$  by eq. (7). In this case  $d_L(z)$  depends on the single parameter  $\Omega_m$  and takes the form

$$d_L(z; \Omega_m)_{th} = c(1+z) \int_0^z \frac{dz^0}{H(z^0; \Omega_m)} \quad (24)$$

Constraints on the parameter  $\Omega_m$  are obtained by the maximum likelihood method [30] which involves the minimization of the  $\chi^2(\Omega_m)$  defined as

$$\chi^2(\Omega_m) = \sum_{i=1}^N \frac{[d_L(z)_{obs} - d_L(z; \Omega_m)_{th}]^2}{\sigma_i^2} \quad (25)$$

where  $N$  is the number of the observed SNIa luminosity distances and  $\sigma_i$  are the corresponding 1- $\sigma$  errors which include errors due to flux uncertainties, internal dispersion of SNIa absolute magnitude and peculiar velocity dispersion. If flatness is not imposed as a prior through eq. (22) then  $d_L(z)_{th}$  depends on two parameters ( $\Omega_m$  and  $\Omega_\Lambda$ ) and the relation between  $d_L(z; \Omega_m; \Omega_\Lambda)_{th}$  and  $H(z; \Omega_m; \Omega_\Lambda)$  takes the form

$$d_L(z)_{th} = \frac{c(1+z)}{\Omega_m + \Omega_\Lambda} \sin \left[ \frac{p}{\Omega_m + \Omega_\Lambda} \int_0^z \frac{dz^0}{H(z^0)} \right] \quad (26)$$

In this case the minimization of eq. (25) leads to constraints on both  $\Omega_m$  and  $\Omega_\Lambda$ . This is the only direct and precise observational probe that can place constraints directly on  $\Omega_m$ . Most other observational probes based on large scale structure observations place constraints on  $\Omega_m$  which are indirectly related to flatness in the context of a flatness prior.

As discussed in section 2 the acceleration of the universe has been confirmed using the above maximum likelihood method since 1998 [1, 2]. Even the early datasets of 1998 [1, 2] were able to rule out the flat matter dominated universe (SCDM:  $\Omega_m = 1, \Omega_\Lambda = 0$ ) at 99% confidence level. The latest datasets are the Gold dataset ( $N = 157$  in the redshift range  $0 < z < 1.75$ ) discussed in section 2 and the first year SNLS (Supernova Legacy Survey) dataset which consists of 71 datapoints in the range  $0 < z < 1$  plus 44 previously published nearby SNIa. The 68% and 95%  $\chi^2$  contours in the ( $\Omega_m$  and  $\Omega_\Lambda$ ) parameter space obtained using the maximum likelihood method are shown in Fig. 11 for the SNLS dataset, a truncated version of the Gold dataset (TG) with  $0 < z < 1$  and the Full Gold (FG) dataset. The following comments can be made on these plots:

The two versions of the Gold dataset favor a closed universe instead of a flat universe ( $\Omega_{tot}^{TG} = 2.16 \pm 0.59, \Omega_{tot}^{FG} = 1.44 \pm 0.44$ ). This trend is not realized by the SNLS dataset which gives  $\Omega_{tot}^{SNLS} = 1.07 \pm 0.52$ .

The point corresponding to SCDM ( $\Omega_m; \Omega_\Lambda$ ) = (1;0) is ruled out by all datasets at a confidence level more than 10  $\sigma$ .

If we use a prior constraint of flatness  $\Omega_m + \Omega_\Lambda = 1$  thus restricting on the corresponding dotted line of Fig. 1 and using the parametrization

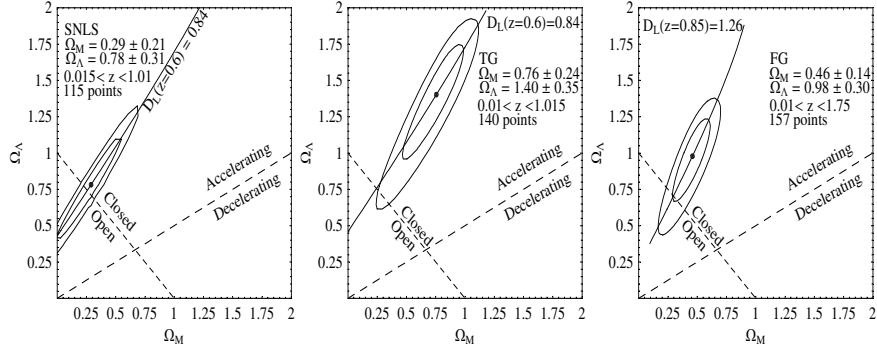


Fig. 11. The 68% and 95%  $\chi^2$  contours in the  $(\Omega_m$  and  $\Omega_\Lambda$ ) parameter space obtained using the SNLS, TG and FG datasets (from Ref. [31]).

$$H(z)^2 = H_0^2 [\Omega_m (1+z)^2 + (1-\Omega_m)] \quad (27)$$

we minimize  $\chi^2(\Omega_m)$  of eq (25)

$$\Omega_m^{SNLS} = 0.26 \pm 0.04 \quad (28)$$

$$\Omega_m^{TG} = 0.30 \pm 0.05 \quad (29)$$

$$\Omega_m^{FG} = 0.31 \pm 0.04 \quad (30)$$

These values of  $\Omega_m$  are consistent with corresponding constraints from the CMB [8] and large scale structure observations[9].

Even though  $\Lambda$ CDM is the simplest dark energy model and is currently consistent with all cosmological observations (especially with the SNLS dataset) the question that may still be address is the following: 'Is it possible to get better fits (lowering  $\chi^2$  further) with different  $H(z)$  parametrizations and if yes what are the common features of these better fits?' The strategy towards addressing this question involves the following steps:

Consider a physical model and extract the predicted recent expansion history  $H(z; a_1; a_2; \dots; a_n)$  as a function of the model parameters  $a_1; a_2; \dots; a_n$ . Alternatively a model independent parametrization for  $H(z; a_1; a_2; \dots; a_n)$  (or equivalently  $w(z; a_1; a_2; \dots; a_n)$ ) may be constructed aiming at the best possible fit to the data with a small number of parameters (usually 3 or less).

Use eq. (7) to obtain the theoretically predicted luminosity distance  $d_L(z; a_1; a_2; \dots; a_n)_{th}$  as a function of  $z$ .

Use the observed luminosity distances  $d_L(z_i)_{obs}$  to construct  $\chi^2$  along the lines of eq. (25) and minimize it with respect to the parameters  $a_1; a_2; \dots; a_n$ .

From the resulting best fit parameter values  $a_1; a_2; \dots; a_n$  (and their error bars) construct the best fit  $H(z; a_1; a_2; \dots; a_n)$ ,  $d_L(z; a_1; a_2; \dots; a_n)$  and  $w(z; a_1; a_2; \dots; a_n)$ . The quality of fit is measured by the depth of the minimum of  $\chi^2$  i.e.  $\chi^2_{\text{min}}(a_1; a_2; \dots; a_n)$ .

Most useful parameterizations reduce to  $\Lambda$ CDM of eq. (21) for specific parameter values giving a  $\chi^2_{\Lambda\text{CDM}}$  for these parameter values. Let

$$\chi^2_{\Lambda\text{CDM}} = \chi^2_{\text{min}}(a_1; a_2; \dots; a_n) - \chi^2_{\Lambda\text{CDM}} \quad (31)$$

The value of  $\chi^2_{\Lambda\text{CDM}}$  is usually negative since  $\chi^2$  is usually further reduced due to the larger number of parameters compared to  $\Lambda$ CDM. For a given number of parameters the value of  $\chi^2_{\Lambda\text{CDM}}$  gives a measure of the probability of having  $\Lambda$ CDM physically realized in the context of a given parameterization [32]. The smaller this probability is, the more 'superior' this parameterization is compared to  $\Lambda$ CDM. For example for a two parameter parameterization and  $j = \chi^2_{\Lambda\text{CDM}} > 2.3$  the parameters of  $\Lambda$ CDM are more than 1 away from the best fit parameter values of the given parameterization. This statistical test has been quantified in Ref. [32] and applied to several  $H(z)$  parameterizations.

As an example let us consider the two parameter polynomial parameterization allowing for dark energy evolution

$$H(z)^2 = H_0^2 [ \omega_m (1+z)^3 + a_2 (1+z)^2 + a_1 (1+z) + (1 - a_2 - a_1 - \omega_m) ] \quad (32)$$

in the context of the Full Gold dataset. Applying the above described  $\chi^2$  minimization leads to the best fit parameter values  $a_1 = 1.67 \pm 1.03$  and  $a_2 = -4.16 \pm 2.53$ . The corresponding  $j = \chi^2_{\Lambda\text{CDM}}$  is found to be 2.9 which implies that the  $\Lambda$ CDM parameter values ( $a_1 = a_2 = 0$ ) are in the range of 1.2 away from the best fit values.

The same analysis can be repeated for various different parameterizations in an effort to identify the common features of the best fit parameterizations. For example two other dynamical dark energy parameterizations used commonly in the literature are defined in terms of  $w(z)$  as

Parameterization A :

$$w(z) = w_0 + w_1 z \quad (33)$$

$$H^2(z) = H_0^2 [ \omega_m (1+z)^3 + (1 - \omega_m) (1+z)^{3(1+w_0+w_1)} e^{3w_1 z} ] \quad (34)$$

Parameterization B :

$$w(z) = w_0 + w_1 \frac{z}{1+z} \quad (35)$$

$$H^2(z) = H_0^2 [ \omega_m (1+z)^3 + (1 - \omega_m) (1+z)^{3(1+w_0+w_1)} e^{3w_1 [1-(1+z)^{-1}]} ] \quad (36)$$

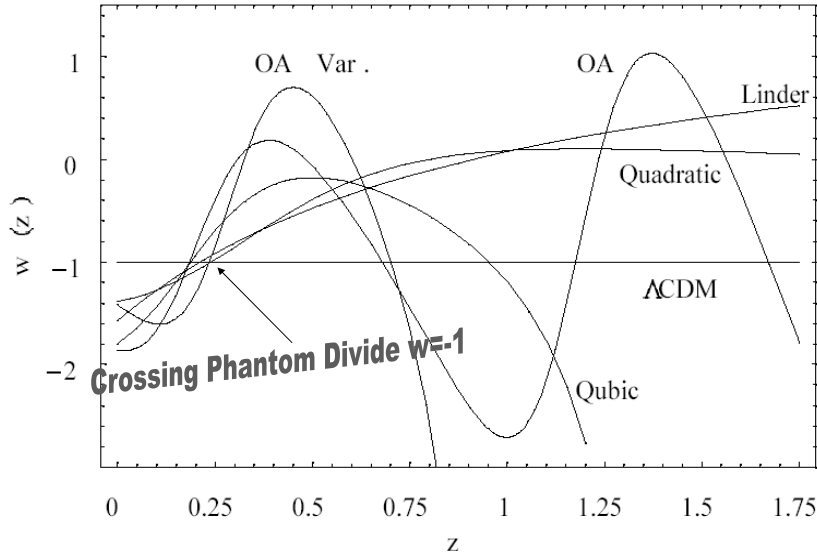


Fig. 12. The best fit forms of  $w(z)$  obtained from a variety of parametrizations [32] in the context of the FullGold dataset. Notice that they all cross the line  $w = -1$  also known as the Phantom Divide Line (PDL).

where the corresponding forms of  $H(z)$  are derived using eq. (17). The best fit forms of  $w(z)$  obtained from a variety of these and other parametrizations [32] in the context of the FullGold dataset are shown in Fig. 12. Even though these best fit forms appear very different at redshifts  $z > 0.5$  (mainly due to the two derivatives involved in obtaining  $w(z)$  from  $d_L(z)$ ), in the range  $0 < z < 0.5$  they appear to have an interesting common feature: they all cross the line  $w = -1$  also known as the Phantom Divide Line (PDL). As discussed in the next section this feature is difficult to reproduce in most theoretical models based on minimally coupled scalar fields and therefore if it persisted in other independent datasets it could be a very useful tool in discriminating among theoretical models. Unfortunately if the same analysis is made in the context of the more recent SNLS dataset it seems that this common feature does not persist. In Fig. 13 the best fit  $w(z)$  (along with the  $1\sigma$  error region) is shown in the context of three different datasets (in analogy with Fig. 11) for the three different parametrizations (A, B and polynomial of eq. (32) (called C in Fig. 13)). Even though the crossing of the PDL is realized at best fit for both the FG and TG datasets it is not realized at best fit when the SNLS is used. Thus we must wait until further SNIa datasets are released before the issue is settled. In Fig. 14 I show the  $1\sigma$  and  $2\sigma$  contours corresponding to parametrizations A and B with a prior of  $\omega_m = 0.24$  confirming the fact that the SNLS dataset provides best fit parameter values that are almost

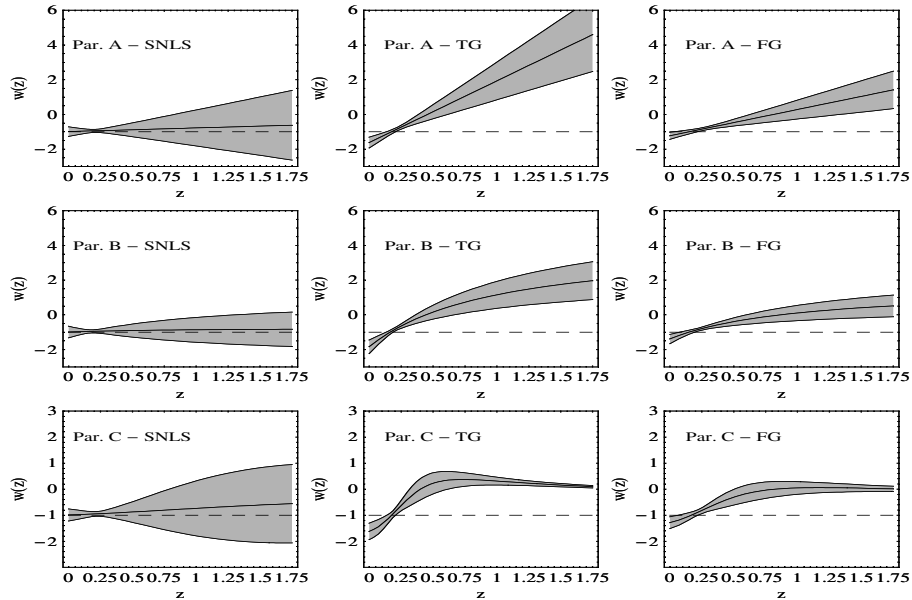


Fig. 13. The best fit  $w(z)$  (along with the  $1\sigma$  error (shaded region)) is shown in the context of three different datasets (in analogy with Fig. 11) for three different parametrizations (A, B and C) [31].

identical to those corresponding to LCDM ( $w_0 = -1, w_1 = 0$ ) despite the dynamical degrees of freedom incorporated in the parametrizations A and B. It should be pointed out however that despite the differences in the best fit parametrizations, the three datasets (SNLS, TG and FG) are consistent with each other at the 95% confidence range (see e.g. Fig. 14) and they are all consistent with flat LCDM with  $\Omega_m \approx 0.3$ .

## 5 Theoretical Models for Dark Energy

Even though LCDM is the simplest model consistent with current cosmological data it is plagued with theoretical fine tuning problems discussed in the previous section (the ‘coincidence’ and the ‘cosmological constant’ problems). In addition dynamical dark energy parametrizations of  $H(z)$  provide in certain cases significantly better fits to the SNIa data. Therefore the investigation of physically motivated models that predict a dynamical evolution of dark energy is an interesting and challenging problem.

The role of dark energy can be played by any physical field with positive energy and negative pressure which violates the strong energy condition ( $\rho + 3p > 0$  ( $w > -\frac{1}{3}$ )). Quintessence scalar fields [33] with small positive kinetic term ( $-1 < w < -\frac{1}{3}$ ) violate the strong energy condition but not the domi-

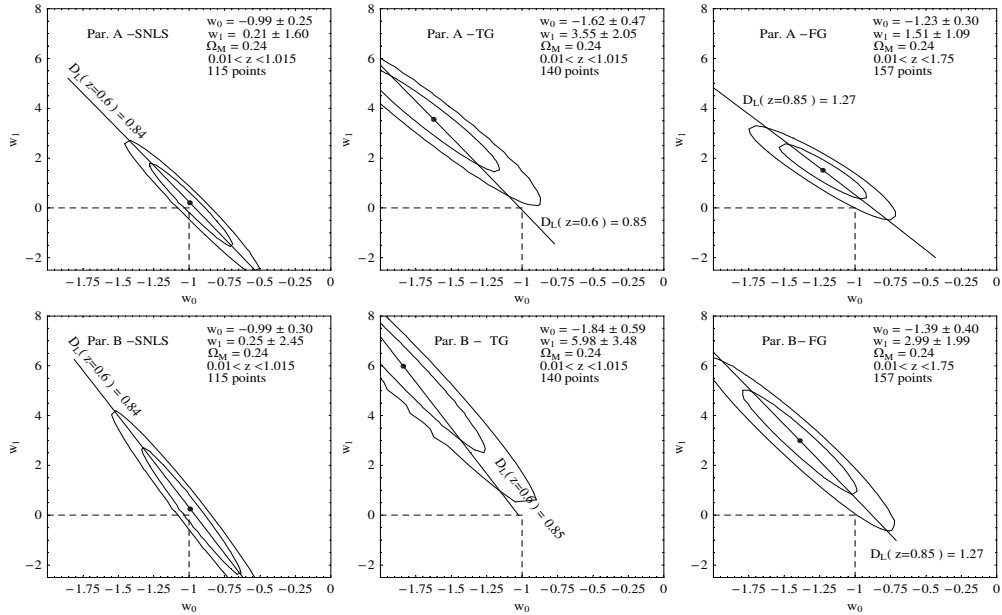


Fig. 14. The 1 and 2 contours corresponding to parametrizations A and B with a prior of  $\Omega_m = 0.24$ . Notice that the SNLS dataset provides best fit parameter values that are almost identical to those corresponding to  $\Lambda$ CDM ( $w_0 = -1, w_1 = 0$ ).

phantom energy condition  $w + p > 0$ . Their energy density scales down with the cosmic expansion and so does the cosmic acceleration rate. Phantom fields [34] with negative kinetic term ( $w < -1$ ) violate the strong energy condition, the dominant energy condition and maybe physically unstable. However, they are also consistent with current cosmological data and according to recent studies [35, 29, 32] they may be favored over their quintessence counterparts.

Homogeneous quintessence or phantom scalar fields are described by Lagrangians of the form

$$L = \frac{1}{2} \dot{\phi}^2 - V(\phi) \quad (37)$$

where the upper (lower) sign corresponds to a quintessence (phantom) field in equation (37) and in what follows. The corresponding equation of state parameter is

$$w = \frac{p}{\rho} = \frac{\frac{1}{2} \dot{\phi}^2 - V(\phi)}{\frac{1}{2} \dot{\phi}^2 + V(\phi)} \quad (38)$$

For quintessence (phantom) models with  $V(\phi) > 0$  ( $V(\phi) < 0$ ) the parameter  $w$  remains in the range  $-1 < w < 1$ . For an arbitrary sign of  $V(\phi)$  the above restriction does not apply but it is still impossible for  $w$  to cross the PDL  $w = -1$  in a continuous manner. The reason is that for  $w = -1$  a zero kinetic term  $\dot{\phi}^2$  is required and the continuous transition from  $w < -1$  to  $w > -1$  (or

vice versa) would require a change of sign of the kinetic term. The sign of this term however is fixed in both quintessence and phantom models. This difficulty in crossing the PDL  $w = -1$  could play an important role in identifying the correct model for dark energy in view of the fact that data favor  $w' < -1$  and furthermore parametrizations of  $w(z)$  where the PDL is crossed appear to be favored over the cosmological constant  $w = -1$  according to the Gold dataset as discussed in the previous section.

It is therefore interesting to consider the available quintessence and phantom scalar field models and compare the consistency with data of the predicted forms of  $w(z)$  among themselves and with arbitrary parametrizations of  $w(z)$  that cross the PDL. This task has been recently undertaken by several authors in the context of testing the predictions of phantom and quintessence scalar field models [35, 36].

As an example we may consider a particular class of scalar field potentials of the form

$$V(\phi) = s \tag{39}$$

where I have followed Ref. [37] and set  $\phi = 0$  at  $V = 0$ . As discussed in section 2 (see also Ref. [37]) the field may be assumed to be frozen ( $\dot{\phi} = 0$ ) at early times due to the large cosmic friction  $H(\dot{\phi})$ . It has been argued [38] that such a potential is favored by anthropic principle considerations because galaxy formation is possible only in regions where  $V(\phi)$  is in a narrow range around  $V = 0$  and in such a range any potential is well approximated by a linear function. In addition such a potential can provide a potential solution to the cosmic coincidence problem [39].

The cosmological evolution in the context of such a model [40] is obtained by solving the coupled Friedmann-Robertson-Walker (FRW) and the scalar field equation

$$\frac{\ddot{a}}{a} = \frac{1}{3M_p^2} (\dot{\phi}^2 + s) - \frac{\Omega_m H_0^2}{2a^3} \tag{40}$$

$$+ 3\frac{\dot{a}}{a} \dot{\phi} - s = 0 \tag{41}$$

where  $M_p = (8\pi G)^{-1/2}$  is the Planck mass and I have assumed a potential of the form

$$V(\phi) = \pm s \tag{42}$$

where the upper (lower) sign corresponds to quintessence (phantom) models. The solution of the system (40)-(41) for both positive and negative values of the single parameter of the models  $s$ , is a straightforward numerical problem [40] which leads to the predicted forms of  $H(z;s)$  and  $w(z;s)$ . These forms may then be fit to the SnIa datasets for the determination of the best fit value of the parameter  $s$ . This task has been undertaken in Ref. [40] using the Full Gold dataset. The best fit value of  $s$  was found to be practically indistinguishable from zero which corresponds to the cosmological constant



for both the quintessence and the phantom cases. The predicted forms of  $w(z)$  for a phantom and a quintessence case and  $s' = 2$  is shown in Fig. 15. The value of  $\chi^2_{\text{LCDM}}$  is positive in both cases which implies that the

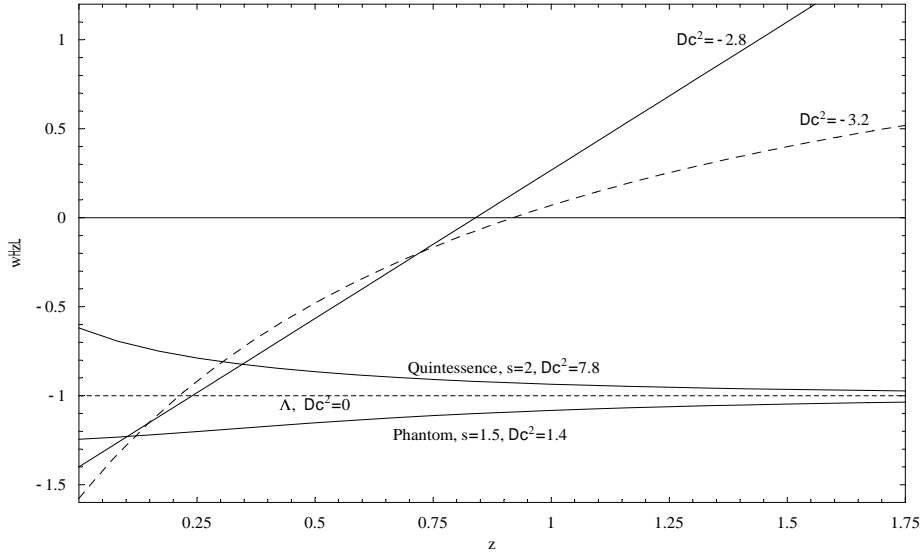


Fig. 15. The predicted forms of  $w(z)$  for a phantom and a quintessence case and  $s' = 2$  provide worse fits to the Gold dataset than LCDM and even worse compared to best fit parameterizations that cross the PDL [40].

It is worse compared to LCDM. The main reason for this is that both the quintessence and phantom minimally coupled scalar field models do not allow for crossing of the PDL line for any parameter value as discussed above. In contrast, the best fit  $w(z)$  parameterizations A and B of eqs. (33)–(35) which allow for PDL crossing have a negative  $\chi^2_{\text{LCDM}}$  in the context of the Gold dataset as shown in Fig. 15 and therefore provide better fits than the field theory models. It should be stressed however that in the context of the SNLS dataset, parameterizations that allow for crossing of the PDL do not seem to have a similar advantage as discussed in the previous section.

The difficulty in crossing the PDL  $w = -1$  described above could play an important role in identifying the correct model for dark energy in view of the fact that data favor  $w' < 1$  and furthermore parameterizations of  $w(z)$  where the PDL is crossed appear to be favored over the cosmological constant  $w = -1$  in the context of the Gold dataset. Even for generalized k-essence Lagrangians [41, 42] of a minimally coupled scalar field eq

$$L = \frac{1}{2} \dot{\phi}^2 - V(\phi) \quad (43)$$

it has been shown [43] to be impossible to obtain crossing of the PDL. Multiple field Lagrangians (combinations of phantom with quintessence fields [44, 45, 46, 47]) have been shown to in principle achieve PDL crossing but such models are complicated and without clear physical motivation (but see [48] for an interesting physically motivated model).

The obvious class of theories that could lead to a solution of the above described problem is the non-minimally coupled scalar fields. Such theories are realized in a universe where gravity is described by a scalar-tensor theory and their study is well motivated for two reasons:

1. A scalar-tensor theory of gravity is predicted by all fundamental quantum theories that involve extra dimensions. Such are all known theories that attempt to unify gravity with the other interactions (eg supergravity (SUGRA), M-theory etc).
2. Scalar fields emerging from scalar tensor theories (extended quintessence) can predict an expansion rate  $H(z)$  that violates the inequality

$$\frac{d(H(z)^2 - H_0^2)}{dz} > 3 \omega_m (1+z)^2 \quad (44)$$

which is equivalent to crossing the PDL with  $w = -1$  (see eg Ref. [49]).

In fact it has been shown in Ref. [49] that in contrast to minimally coupled quintessence, scalar tensor theories can reproduce the main features of the best fit Hubble expansion history obtained from the Gold dataset. However, the precise determination of the scalar tensor theory potentials requires more accurate SNIa data and additional cosmological observational input.

## 6 The Fate of a Phantom Dominated Universe: Big Rip

As discussed in section 4 the Gold dataset favors a dynamical dark energy with present value of the equation of state parameter  $w$  in the phantom regime. If this trend is verified by future datasets and if  $w$  remains in the phantom regime in the future then the fate of the universe acquires novel interesting features. The energy density of phantom fields increases with time and so does the predicted expansion acceleration rate  $\frac{\ddot{a}}{a}$ . This monotonically increasing acceleration rate of the expansion may be shown to lead to a novel kind of singularity which occurs at a finite future time and is characterized by divergences of the scale factor  $a$ , the Hubble parameter  $H$  its derivative  $\dot{H}$  and the scalar curvature. This singularity has been called 'Big Smash' [50] the first time it was discussed and 'Big Rip' [51] in a more recent study. An immediate consequence of the very rapid expansion rate as the Big Rip singularity is approached is the dissociation of bound systems due to the buildup of repulsive negative pressure in the interior of these systems.

This dissociation of bound systems can be studied by considering the spacetime in the vicinity of a point mass  $M$  placed in an expanding background in order to study the effects of the cosmic expansion on bound systems. Such a metric should interpolate between a static Schwarzschild metric at small distances from  $M$  and a time dependent Friedmann spacetime at large distances. In the Newtonian limit (weak field, low velocities) such an interpolating metric takes the form [52]:

$$ds^2 = \left(1 - \frac{2GM}{a(t)}\right) dt^2 - a(t)^2 (dr^2 + \sin^2 r d\Omega^2) \tag{45}$$

where  $r$  is the comoving radial coordinate. Using

$$r = a(t) \tag{46}$$

the geodesics corresponding to the line element (45) take the form

$$\left(r - \frac{a}{a}\right) \frac{GM}{r^2} + r'^2 = 0 \tag{47}$$

and

$$r'^2 = L \tag{48}$$

where  $L$  is the constant angular momentum per unit mass. Therefore the radialequation of motion for a test particle in the Newtonian limit considered is

$$r = \frac{a}{a}r + \frac{L^2}{r^3} - \frac{GM}{r^2} \tag{49}$$

The first term on the rhs proportional to the cosmic acceleration is a time dependent repulsive term which is increasing with time for  $w < -1$ . This is easy to see by considering the Friedmann equation (12) combined with the dark energy evolution  $\dot{\rho}_x = -3(1+w)\rho_x$  where the scale factor obtained from the Friedmann equation is

$$a(t) = \frac{a(t_m)}{[w + (1+w)(t-t_m)]^{\frac{2}{3(1+w)}}} \text{ for } t > t_m \tag{50}$$

and  $t_m$  is the transition time from decelerating to accelerating expansion. For phantom energy ( $w < -1$ ) the scale factor diverges at a finite time

$$t = \frac{w}{1+w} t_m > 0 \tag{51}$$

leading to the Big Rip singularity. Clearly, the time dependent repulsive term of eq. (49) diverges at the Big Rip singularity.

A quantitative analysis [53] shows that the geodesic equation (49) is equivalent to a Newtonian equation with a time-dependent effective potential that determines the dynamics of the bound system which in dimensionless form is [53]

$$V_{eff} = \frac{\dot{l}_0^2}{r} + \frac{\dot{l}_0^2}{2r^2} - \frac{1}{2} (\dot{t})^2 r^2 \quad (52)$$

where

$$\dot{t} = \frac{p \sqrt{2j_l + 3w_j}}{3(w + (1+w)t)} \quad (53)$$

with  $w < 1$  and  $\dot{l}_0$  is defined as

$$\dot{l}_0^2 = \frac{GM}{r_0^3} t_m^2 \quad (54)$$

At  $t = 1$  the system is assumed to be in circular orbit with radius given by the minimum  $r_{min}(t)$  of the effective potential of equation (52). It is easy to show that the minimum of the effective potential (52) disappears at a time  $t_{rip}$  which obeys

$$t_{rip} = \frac{16}{9} \frac{p \sqrt{2j_l + 3w_j}}{6j_l + w_j} \quad (55)$$

The value of the bound system dissociation time  $t_{rip}$  may be verified by numerically solving the geodesic Newtonian equation of a test particle with the effective potential (52). The resulting evolution close to the predicted dissociation time  $t_{rip}$  is shown in Fig. 16 for  $w = 1.2$  and verifies the dissociation time predicted by equation (55). Using the appropriate values for the bound

Table 2. The difference between dissociation times  $t_{rip}$  and the big rip time  $t$  for three bound systems in years as predicted by equation (55). The dissociation times  $t_{rip}$  for the three bound systems in units of  $t_m$  are also shown in column 3. The value  $w = 1.2$  was assumed [53].

System	$t - t_{rip}$ (yrs)	$t_{rip} = t_m$
Solar System	$1.88 \cdot 10^4$	6.00
Milky Way	$3.59 \cdot 10^8$	5.94
Coma Cluster	$1.58 \cdot 10^{10}$	3.19

system masses  $M$  the dissociation times of cosmological bound systems may be obtained. These are shown in Table 2.

## 7 Future Prospects-Conclusion

The question of the physical origin and dynamical evolution properties of dark energy is the central question currently in cosmology. Since the most sensitive and direct probes towards the answer of this question are distance-redshift surveys of Sn Ia there has been intense activity during the recent years towards designing and implementing such projects using ground based and satellite observatories. Large arrays of CCDs such as M O S A I C camera at Cerro Tololo

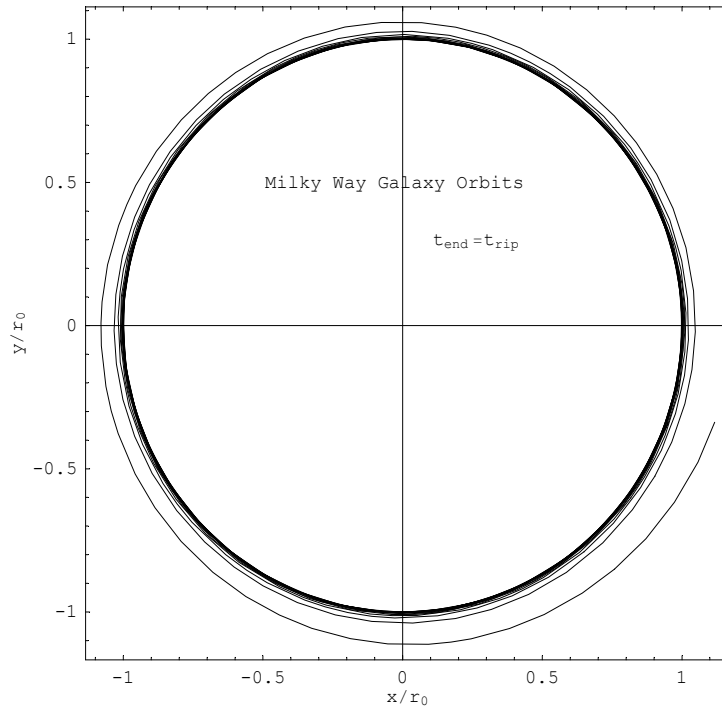


Fig. 16. The numerically obtained evolution of a galactic size two body system at times close to the predicted dissociation time  $t_{rip}$  [53].

Inter-American Observatory, the SUPRIME camera at Subaru or the MEGA-CAM at the Canada-France-Hawaii Telescope (CFHT) are some of the best ground based tools for supernova searches. These devices work well in the reddest bands (800–900nm) where the ultraviolet and visible light of redshifted high- $z$  SNIa is detected. Searches from the ground have the advantages of large telescope apertures (Subaru for example has 10 times the collecting area of the Hubble Space Telescope (HST)) and large CCD arrays (the CFHT has a 378-million pixel camera compared to the Advanced Camera for Surveys on HST which has 16 million pixels). On the other hand the advantage of space satellite observatories like the HST include avoiding the bright and variable night-sky encountered in the near infrared, the potential for much sharper imaging for point sources like supernovae to distinguish them from galaxies

in which they reside and better control over the observing conditions which need not factor in weather and moonlight.

The original two SNIa search teams (the Supernova Cosmology Project and the High-z Supernova Search Team) have evolved to a number of ongoing and proposed search projects both satellite and ground based. These projects

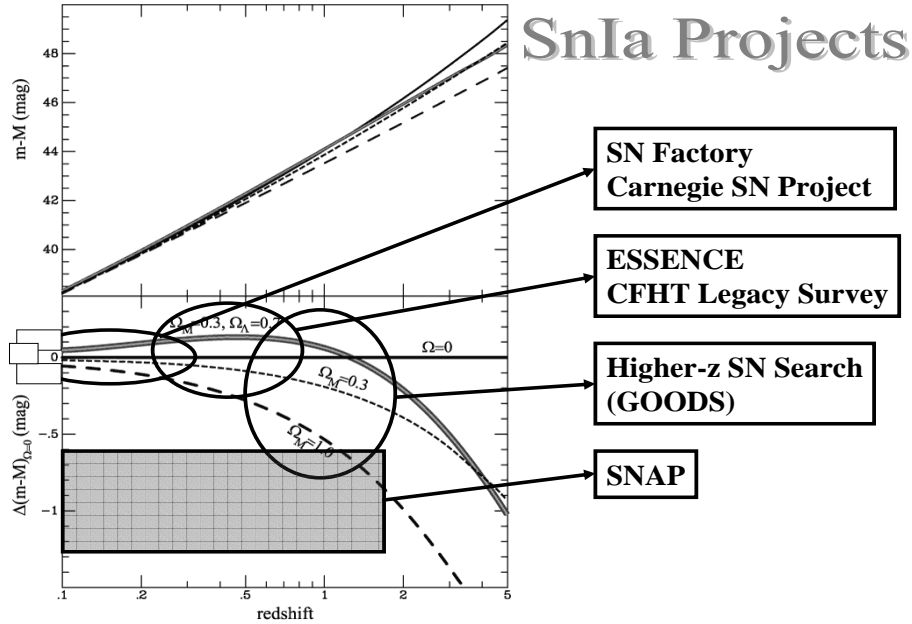


Fig. 17. Ongoing and proposed SNIa search projects with the corresponding redshift ranges.

(see Fig. 17) include the following:

The Higher-z Supernova Search Team (H Z T) [54] and the G O O D S [55] team of H S T : This has originated from the High-z Supernova Search Team and has A . R i e s s of Space Telescope Sci. Inst. as its team leader. This team is in collaboration with the G O O D S program (G r e a t O b s e r v a t o r i e s O r i g i n D e e p S u r v e y) using the ACS of the H S T to detect and analyze high redshift ( $0.5 < z < 2$ ) SNIa. Successive G O O D S observations are spaced by 45 days providing 5 epochs of data on two fields: the Hubble Deep Field (HDF) north and south. Whereas the G O O D S team adds these images to build a superdeep field, the H Z T subtracts the accumulated template image from each incoming frame. Thus the H Z T has already detected more than 42 supernovae in the above redshift range.

Equation of State: Supernovae trace Cosmic Expansion (E S S E N C E) [56]: This has also originated from the High-z Supernova Search Team and has C . S t u b b s of the Univ. of Washington, C . S m i t h and N . S u n t z e of Cerro

Toledo as its team leader. This ongoing program aims to find and measure 200 SNIa's in the redshift range of  $0.15 < z < 0.7$  where the transition from decelerating to accelerating expansion occurs. Spectroscopic backup to the program comes from the ground based Gemini, Magellan, VLT, Keck and MMT Observatories. The ESSENCE project is a five-year endeavor, with the goal of tightly constraining the time average of the equation-of-state parameter  $w = p/\rho$  of the dark energy. To help minimize systematic errors, all of their ground-based photometry is obtained with the same telescope and instrument. In 2003 the highest-redshift subset of ESSENCE supernovae was selected for detailed study with HST.

The Supernova Legacy Survey (SNLS) [57]: The CFHT Legacy Survey aims at detecting and monitoring about 1000 supernovae in the redshift range  $0 < z < 1$  with Megaprime at the Canada-France-Hawaii telescope between 2003 and 2008. High- $z$  spectroscopy of SNIa is being carried on 8m class telescopes (Gemini, VLT, Keck). Team representatives are: C. Pritchet (Univ. Victoria), P. Astier (CNRS/IN2P3), S. Basa (CNRS/INSU) et. al. The SNLS has recently released the first year dataset [6].

Nearby Supernova Factory (SNF) [58]: The Nearby Supernova Factory (SNF) is an international collaboration based at Lawrence Berkeley National Laboratory. Greg Aldering of Berkeley Lab's Physics Division is the principal investigator of the SNF. The goal of the SNF is to discover and carefully study 300 to 600 nearby Type Ia supernovae in the redshift range  $0 < z < 0.3$ .

Carnegie SN Project (CSP) [59]: The goal of the project is the comprehensive study of both Type Ia and II Supernovae in the local ( $z < 0.07$ ) universe. This is a long-term program with the goal of obtaining exceedingly-well calibrated optical/near-infrared light curves and optical spectroscopy of over 200 Type Ia and Type II supernovae. The CSP takes advantage of the unique resources available at the Las Campanas Observatory (LCO). The team leader is R. Carlberg (Univ. of Toronto).

Supernova Acceleration Probe (SNAP) [60]: This is a proposed space mission originating from LBNL's Supernova Cosmology Project that would increase the discovery rate for SNIa's to about 2000 per year. The satellite called SNAP (Supernova / Acceleration Probe) would be a space based telescope with a one square degree field of view with 1 billion pixels. The project schedule would take approximately four years to construct and launch SNAP, and another three years of mission observations. SNAP has a 2 meter telescope with a large field of view: 600 times the sky area of the Hubble Space Telescopes Wide Field Camera. By repeatedly imaging 15 square degrees of the sky, SNAP will accurately measure the energy spectra and brightness over time for over 2,000 Type Ia supernovae, discovering them just after they explode.

These projects aim at addressing important questions related to the physical origin and dynamical properties of dark energy. In particular these questions can be structured as follows:

Can the accelerating expansion be attributed to a dark energy ideal fluid with negative pressure or is it necessary to implement extensions of GR to understand the origin of the accelerating expansion?

Is  $w$  evolving with redshift and crossing the PDL? If the crossing of the PDL by  $w(z)$  is confirmed then it is quite likely that extensions of GR will be required to explain observations.

Is the cosmological constant consistent with data? If it remains consistent with future more detailed data then the theoretical efforts should be focused on resolving the coincidence and the cosmological constant problems which may require anthropic principle arguments.

The main points of this brief review may be summarized as follows:

Dark energy with negative pressure can explain SNIa cosmological data indicating accelerating expansion of the universe.

The existence of a cosmological constant is consistent with SNIa data but other evolving forms of dark energy crossing the  $w = -1$  line may provide better fits to some of the recent data (Gold dataset).

New observational projects are underway and are expected to lead to significant progress in the understanding of the properties of dark energy.

## References

1. S. Perlmutter et al, *Nature* (London) 391, 51 (1998);
2. Riess A et al, *Astron. J.* 116 1009 (1998);
3. Tonry, J L et al., 2003 *Astroph. J.* 594 1;
4. Perlmutter S J et al., *Astroph. J.* 517 565 (1999); Barris, B et al., 2004 *Astroph. J.* 602 571; Knop R et al., 2003 *Astroph. J.* 598 102;
5. A. G. Riess et al. [Supernova Search Team Collaboration], *Astrophys. J.* 607, 665 (2004).
6. P. Astier et al., *arXiv astro-ph/0510447*.
7. V. Sahni, *arXiv astro-ph/0403324*.
8. D. Spergel et al., *Astrophys. J. Suppl.* 148 (2003) 175, [*arXiv astro-ph/0302209*]
9. M. Tegmark et al, *Phys. Rev. D* 69 (2004) 103501, [*astro-ph/0310723*]
10. V. Sahni and A. A. Starobinsky, *Int. J. Mod. Phys. D* 9, 373 (2000) [*arXiv astro-ph/9904398*].
11. P. J. Peebles and B. Ratna, *Astrophys. J.* 325, L17 (1988); R. R. Caldwell, R. Dave and P. J. Steinhardt, *Phys. Rev. Lett.* 80, 1582 (1998) [*arXiv astro-ph/9708069*]; I. Zlatev, L. M. Wang and P. J. Steinhardt, *Phys. Rev. Lett.* 82, 896 (1999).
12. V. Sahni and L. M. Wang, *Phys. Rev. D* 62, 103517 (2000) [*arXiv astro-ph/9910097*].



13. F. Perrotta, C. Baccigalupi and S. Matarrese, *Phys. Rev. D* 61, 023507 (2000) [[arXiv:astro-ph/9906066](#)]; A. Riazuelo and J. P. Uzan, *Phys. Rev. D* 66, 023525 (2002) [[arXiv:astro-ph/0107386](#)]; G. E. Sposito-Farese and D. Polarski, *Phys. Rev. D* 63, 063504 (2001) [[arXiv:gr-qc/0009034](#)].
14. D. F. Torres, *Phys. Rev. D* 66, 043522 (2002) [[arXiv:astro-ph/0204504](#)].
15. S. Nojiri and S. D. Odintsov, [arXiv:hep-th/0308176](#).
16. A. Y. Kamenshchik, U. Moschella and V. Pasquier, *Phys. Lett. B* 511, 265 (2001) [[arXiv:gr-qc/0103004](#)].
17. K. Freese and M. Lewis, *Phys. Lett. B* 540, 1 (2002) [[arXiv:astro-ph/0201229](#)].
18. L. Perivolaropoulos and C. Sourdis, *Phys. Rev. D* 66, 084018 (2002) [[arXiv:hep-ph/0204155](#)]; M. Sami, N. Savchenko and A. Toporensky, *Phys. Rev. D* 70, 123528 (2004) [[arXiv:hep-th/0408140](#)]; T. R. Mangan, *Gen. Rel. Grav.* 33, 1415 (2001) [[arXiv:gr-qc/0103021](#)].
19. L. Perivolaropoulos, *Phys. Rev. D* 67, 123516 (2003) [[arXiv:hep-ph/0301237](#)].
20. V. Sahni and Y. Shtanov, *JCAP* 0311, 014 (2003) [[arXiv:astro-ph/0202346](#)].
21. R. R. Caldwell, *Phys. Lett. B* 545, 23 (2002) [[arXiv:astro-ph/9908168](#)].
22. Edward W. Kolb, Michael S. Turner: *The Early Universe*, (*Frontiers in Physics* 1990).
23. G. H. Jacoby et al., *Pub. Astron. Soc. Pac.* 104, 599 (1992); S. van den Bergh, *Pub. Astron. Soc. Pac.* 104, 861 (1992); S. van den Bergh, *Pub. Astron. Soc. Pac.* 106, 1113 (1994); M. Fukugita, C. J. Hogan, and P. J. E. Peebles, *Nature* 366, 309 (1993); A. Sandage and G. Tammann, in *Critical Dialogues in Cosmology*, ed. N. Turok (Perinceton, 1997), [astro-ph/9611170](#); W. Freedman, *ibid.*, [astro-ph/9612024](#); C. J. Hogan, <http://pdg.lbl.gov/1998/hubbleexp.pdf> (1997).
24. S. Perlmutter, et al., 1995. in *Presentations at the NATO ASI in Aguilafava, Spain*, LBL-38400, page I.1, and in *Thermonuclear Supernova*, P. Ruiz-Lapuente, R. Canal, and J. Isern, eds. (Dordrecht: Kluwer, 1997).
25. A. Kin, A. Goobar and S. Perlmutter, *Publ. Astron. Soc. Pac.* 108, 190 (1996) [[arXiv:astro-ph/9505024](#)].
26. S. Perlmutter et al., *Astrophys. J.* 483, 565 (1997).
27. A. N. Aguirre, *Astrophys. J.* 512, L19 (1999) [[arXiv:astro-ph/9811316](#)]; A. N. Aguirre, *Astrophys. J.*, 512, L19-L22, (1999).
28. D. Huterer and M. S. Turner, *Phys. Rev. D* 64, 123527 (2001) [[arXiv:astro-ph/0012510](#)].
29. S. Nesseris and L. Perivolaropoulos, *Phys. Rev. D* 70, 043531 (2004) [[arXiv:astro-ph/0401556](#)].
30. W. H. Press et al., *Numerical Recipes*, Cambridge University Press (1994).
31. S. Nesseris and L. Perivolaropoulos, [arXiv:astro-ph/0511040](#).
32. R. Lazkoz, S. Nesseris and L. Perivolaropoulos, [arXiv:astro-ph/0503230](#).
33. B. Ratra and P. J. E. Peebles, *Phys. Rev. D* 37, 3406 (1988); *Rev. Mod. Phys.* 75, 559 (2003) [[arXiv:astro-ph/0207347](#)]; C. Wetterich, *Nucl. Phys. B* 302, 668 (1988); P. G. Ferreira and M. Joyce, *Phys. Rev. D* 58, 023503 (1998).
34. R. R. Caldwell, *Phys. Lett. B* 545, 23 (2002) [[arXiv:astro-ph/9908168](#)]; P. Singh, M. Sami and N. Dadhich, *Phys. Rev. D* 68, 023522 (2003) [[arXiv:hep-th/0305110](#)]; V. B. Johri, *Phys. Rev. D* 70, 041303 (2004) [[arXiv:astro-ph/0311293](#)]; M. Sami and A. Toporensky, *Mod. Phys. Lett. A* 19, 1509 (2004) [[arXiv:gr-qc/0312009](#)].
35. U. Alam, V. Sahni, T. D. Saini and A. A. Starobinsky, *Mon. Not. Roy. Astron. Soc.* 354, 275 (2004) [[arXiv:astro-ph/0311364](#)]; Y. Wang and P. Mukherjee, *Astrophys. J.* 606, 654 (2004) [[arXiv:astro-ph/0312192](#)]; D. Huterer and A. Cooray,

- Phys. Rev. D 71, 023506 (2005) [arXiv:astro-ph/0404062]; R. A. Daly and S. G. Djorgovski, *Astrophys. J.* 597, 9 (2003) [arXiv:astro-ph/0305197]; R. A. Daly and S. G. Djorgovski, arXiv:astro-ph/0512576.
36. M. C. Bento, O. Bertolami, N. M. C. Santos and A. A. Sen, *Phys. Rev. D* 71, 063501 (2005) [arXiv:astro-ph/0412638]; J. Q. Xia, G. B. Zhao, B. Feng, H. Li and X. Zhang, arXiv:astro-ph/0511625; U. Alam and V. Sahni, arXiv:astro-ph/0511473; H. K. Jassal, J. S. Bagla and T. Padmanabhan, *Phys. Rev. D* 72, 103503 (2005) [arXiv:astro-ph/0506748]; V. B. Johri and P. K. Rath, arXiv:astro-ph/0510017; H. Li, B. Feng, J. Q. Xia and X. Zhang, arXiv:astro-ph/0509272; X. Zhang and F. Q. Wu, *Phys. Rev. D* 72, 043524 (2005) [arXiv:astro-ph/0506310]; R. Opher and A. Pelinson, arXiv:astro-ph/0505476; D. Jain, J. S. Alcaniz and A. Dev, arXiv:astro-ph/0409431.
37. J. Garriga, L. Pogosian and T. Vachaspati, *Phys. Rev. D* 69, 063511 (2004) [arXiv:astro-ph/0311412].
38. J. Garriga and A. Vilenkin, *Phys. Rev. D* 61, 083502 (2000) [arXiv:astro-ph/9908115]; J. Garriga and A. Vilenkin, *Phys. Rev. D* 67, 043503 (2003) [arXiv:astro-ph/0210358]; J. Garriga, A. Linde and A. Vilenkin, *Phys. Rev. D* 69, 063521 (2004) [arXiv:hep-th/0310034].
39. P. P. Avelino, arXiv:astro-ph/0411033.
40. L. Perivolaropoulos, *Phys. Rev. D* 71, 063503 (2005) [arXiv:astro-ph/0412308].
41. C. Amendari-Picon, V. Mukhanov and P. J. Steinhardt, *Phys. Rev. D* 63, 103510 (2001) [arXiv:astro-ph/0006373]; R. J. Scherrer, *Phys. Rev. Lett.* 93, 011301 (2004) [arXiv:astro-ph/0402316].
42. A. Melchiorri, L. Mersini, C. J. Odman and M. Trodden, *Phys. Rev. D* 68, 043509 (2003) [arXiv:astro-ph/0211522].
43. A. Vikman, *Phys. Rev. D* 71, 023515 (2005) [arXiv:astro-ph/0407107].
44. Z. K. Guo, Y. S. Piao, X. M. Zhang and Y. Z. Zhang, arXiv:astro-ph/0410654; B. Feng, X. L. Wang and X. M. Zhang, *Phys. Lett. B* 607, 35 (2005) [arXiv:astro-ph/0404224]; B. Feng, M. Li, Y. S. Piao and X. Zhang, arXiv:astro-ph/0407432; X. F. Zhang, H. Li, Y. S. Piao and X. M. Zhang, arXiv:astro-ph/0501652.
45. R. R. Caldwell and M. Doran, arXiv:astro-ph/0501104.
46. W. Hu, *Phys. Rev. D* 71, 047301 (2005) [arXiv:astro-ph/0410680].
47. H. Stefancic, arXiv:astro-ph/0504518.
48. S. Nojiri, S. D. Odintsov and M. Sasaki, arXiv:hep-th/0504052; B. M. N. Carter and I. P. Neupane, arXiv:hep-th/0510109.
49. L. Perivolaropoulos, *JCAP* 0510, 001 (2005) [arXiv:astro-ph/0504582]; S. Tsuchikawa, *Phys. Rev. D* 72, 083512 (2005) [arXiv:astro-ph/0508542].
50. B. M. Clines, *JHEP* 0208, 029 (2002) [arXiv:hep-th/0112066].
51. R. R. Caldwell, M. Kamionkowski and N. N. Weinberg, *Phys. Rev. Lett.* 91, 071301 (2003) [arXiv:astro-ph/0302506].
52. G. C. McVittie, *MNRAS* 93, 325 (1933).
53. S. Nesseris and L. Perivolaropoulos, *Phys. Rev. D* 70, 123529 (2004) [arXiv:astro-ph/0410309].
54. L. G. Strolger et al., *Astrophys. J.* 613, 200 (2004) [arXiv:astro-ph/0406546].
55. M. G. Ivalisco [The GOODS Team Collaboration], arXiv:astro-ph/0309105.
56. J. Sollerman et al., arXiv:astro-ph/0510026.
57. N. Palanque-Delebrouille [SNLS Collaboration], arXiv:astro-ph/0509425.

58. W . M . Wood-Vasey et al., *New Astron. Rev.* 48, 637 (2004) [arXiv:astro-ph/0401513].
59. W . L. Freedman [The Carnegie Supernova Project Collaboration], arXiv:astro-ph/0411176.
60. G . Aldering [SNAP Collaboration], arXiv:astro-ph/0209550.